

On the redshift cut-off for steep-spectrum radio sources

Matt J. Jarvis^{1,2*}, Steve Rawlings¹, Chris J. Willott¹,
Katherine M. Blundell¹, Steve Eales³ and Mark Lacy^{1,4,5}

¹*Astrophysics, Department of Physics, Keble Road, Oxford, OX1 3RH, UK*

²*Sterrewacht Leiden, Postbus 9513, 2300 RA Leiden, the Netherlands*

³*Department of Physics and Astronomy, University of Wales College of Cardiff, P.O. Box 913, Cardiff, CF2 3YB, UK*

⁴*Institute of Geophysics and Planetary Physics, L-413 Lawrence Livermore National Laboratory, Livermore, CA 94550, USA*

⁵*Department of Physics, University of California, 1 Shields Avenue, Davis CA 95616, USA*

29 October 2018

ABSTRACT

We use three samples (3CRR, 6CE and 6C*) selected at low radio frequency to constrain the cosmic evolution in the radio luminosity function (RLF) for the ‘most luminous’ steep-spectrum radio sources. Although intrinsically rare, such sources give the largest possible baseline in redshift for the complete flux-density-limited samples currently available. Using parametric models to describe the RLF which incorporate distributions in radio spectral shape and linear size as well as the usual luminosity and redshift, we find that the data are consistent with a constant comoving space density between $z \sim 2.5$ and $z \sim 4.5$. We find this model is favoured over a model with similar evolutionary behaviour to that of optically-selected quasars (i.e. a roughly Gaussian distribution in redshift) with a probability ratio of $\sim 25:1$ and $\sim 100:1$ for spatially-flat cosmologies with $\Omega_\Lambda = 0$ and $\Omega_\Lambda = 0.7$ respectively. Within the uncertainties, this evolutionary behaviour may be reconciled with the shallow decline preferred for the comoving space density of flat-spectrum sources by Dunlop & Peacock (1990) and Jarvis & Rawlings (2000), in line with the expectations of Unified Schemes.

Key words: galaxies:active - galaxies:luminosity function, mass function - radio continuum:galaxies

1 INTRODUCTION

Speculation concerning the cosmic evolution of the radio source population has been at the forefront of astrophysical research since the 1960s. It soon became clear that the radio luminosity function (RLF) declines steeply towards high radio luminosities, and that the (comoving) space densities of the rarest, most luminous quasars and radio galaxies were much higher at epochs corresponding to $z \sim 2$ than they are now (Longair 1966). As emphasised by Peacock (1985), Dunlop & Peacock (1990; hereafter DP90), Shaver et al. (1996; hereafter SH96), Jarvis & Rawlings (2000; hereafter JR00) and many others the crucial advantage of any radio-based work is that with sufficient optical follow-up, it can be made free of optical selection effects, such as increasing dust obscuration at high redshift.

The term ‘redshift cut-off’ made an early appear-

ance in the literature (e.g. Sandage 1972), and is now taken to mean any significant decline in the space density over $2.5 \lesssim z \lesssim 5$. Peacock (1985) and then DP90, found evidence for a redshift cut-off in the distribution of flat-spectrum radio quasars over the redshift range 2 – 4. Through failing to find any flat-spectrum radio quasars at $z > 5$ in a survey covering ~ 4 sr, SH96 (see also Shaver et al. 1998; hereafter SH98) argued for a drop in space density between $2.5 \lesssim z \lesssim 6$ of more than 1 dex. JR00 re-addressed this question using a similar sample to the flat-spectrum sample of SH96/SH98. By considering the effects of a distribution in spectral index and also the presence of any curvature in the radio spectra, JR00 found evidence for a decline between $2.5 \leq z \leq 5$ by a factor ~ 4 in agreement with DP90, although they found that steeper declines such as that preferred by SH96, as well as models invoking a constant comoving space density at high redshift, can only be ruled out at the 90% confidence level with the surveys currently available.

* Email: jarvis@strw.leidenuniv.nl

DP90 also claimed the first evidence for a similar redshift cut-off in the steep-spectrum radio population. According to simple Unified Schemes (e.g. Barthel 1989; Antonucci 1993) steep-spectrum radio sources are the parent, unbeamed, population for Doppler-boosted flat-spectrum objects, and should show similar evolutionary behaviour (Jackson & Wall, 1999)[†]. However, the high selection frequency (2.7 GHz) of the steep-spectrum samples used by DP90 meant that their survey was sensitive to only the most luminous sources at high redshift, an effect which is made more pronounced by the positive correlations between spectral index and redshift/radio luminosity (e.g. Blundell, Rawlings & Willott 1999). The necessity of considering the effects of the distribution in radio spectral parameters, highlighted by JR00 for the flat-spectrum population, is especially acute for this population which typically have steep and curved spectra. There are also worries about the incompleteness of the faint radio-selected sample used by DP90 (see their Appendix A). Moreover, DP90 were forced to use photometric redshift estimates for most of their high-redshift steep-spectrum objects, and since these were based on the still poorly-understood $K - z$ diagram for radio galaxies (e.g. Eales et al. 1997; Jarvis et al. 2001b), this leads to considerable uncertainty in their results.

To ameliorate these problems, our group has been seeking spectroscopic redshifts for samples selected at low radio frequency from the 6C and 7C catalogues (see e.g. Rawlings et al. 1998). There are now three low-frequency-selected samples with essentially complete redshift information: 3CRR (Laing, Riley & Longair, 1983); 6CE (Eales et al. 1985; Rawlings, Eales & Lacy, 2001) and the 7C redshift survey (7CRS; Blundell et al. in prep.; Willott et al. in prep.). Investigation of the RLF of steep-spectrum quasars (Willott et al. 1998), the first of its kind, found no definitive evidence for a redshift cut-off, albeit with only a small sample of quasars. Using the combined 3CRR, 6CE and 7CRS dataset, comprising 357 sources, Willott et al. (2001) obtained similar results for the entire low-frequency population.

In this paper we focus on whether there is any evidence for a redshift cut-off in the space density of the most radio-luminous steep-spectrum radio sources. Our work on follow-up spectroscopy of the 6CE (Rawlings et al. 2001) and 6C* (Blundell et al. 1998; Jarvis et al. 2001a, 2001b) samples provides redshifts for well defined samples containing the distant counterparts of the most luminous radio sources in the 3CRR survey (Laing, Riley & Longair 1983). This analysis of the RLF is different from that by Willott et al. (2001) since it

also includes 6C*, which is crucial in sampling to high redshift.

In Sec. 2 we summarise the relevant properties of the 3CRR, 6CE and 6C* samples, and describe how the most luminous radio sources have been drawn from them. In Sec. 3 we highlight the reasons for concentrating on just the most radio-luminous sources and in Sec. 4 we describe the parametric models used in a maximum likelihood analysis which yield estimates of the RLF. We use the banded V/V_{\max} statistic in Sec. 5 to compare our parametric modelling with a non-parametric approach and in Sec. 6 we compare our predicted redshift distributions with the data and highlight the importance of small number statistics. In Sec. 7 we discuss our results in the context of unified schemes of radio AGN.

We assume $H_0 = 50 \text{ km s}^{-1} \text{ Mpc}^{-1}$, and obtain all results in two spatially-flat cosmologies ($\Omega_M = 1$ and $\Omega_\Lambda = 0$, hereafter cosmology I and $\Omega_M = 0.3$ and $\Omega_\Lambda = 0.7$, hereafter cosmology II). We use the convention for spectral index α that $S_\nu \propto \nu^{-\alpha}$ and $\alpha_{\nu_1}^{\nu_2}$ represents the spectral index between observed frequencies ν_1 and ν_2 . All luminosities quoted are measured in units of $\text{W Hz}^{-1} \text{sr}^{-1}$ at rest-frame 151 MHz unless stated otherwise.

2 COMPLETE SAMPLES OF RADIO SOURCES SELECTED AT LOW FREQUENCY

2.1 The advantages of using three samples

Flux-density-limited samples over a particular sky area provide a direct way of constraining the RLF if they have complete redshift information. In this analysis, in which only the ‘most luminous’ sources are considered, the 7CRS with a flux-density limit $S_{151} \geq 0.5 \text{ Jy}$ covering a total sky area of 0.022 sr would contribute only one such source, principally due to the small sky area it surveyed and the steepness of the RLF (see Willott et al. 2001). Thus, inclusion of 7CRS was deemed unnecessary for the purpose of this paper and we only use three samples, 3CRR, 6CE and 6C* which we describe in the next three sections.

2.2 3CRR

We use the 3CRR sample of Laing, Riley & Longair (1983), which contains 173 sources. Following Blundell et al. (1999) we exclude 3C 231 (M82) since the radio emission is a consequence of star-formation (Condon et al. 1990) rather than an active nucleus. Two other sources are also excluded (3C 345 and 3C 454.3) because their emission only exceeds the 178 MHz flux-density limit because of Doppler boosting of their core emission. The sample has 100% spectroscopic redshifts.

[†] JR00 have also suggested that Giga-Hertz Peaked Spectrum (GPS) sources also play a major role in the flat-spectrum surveys along with Doppler Boosted sources, particularly at the high luminosity end of the RLF.

Sample	Flux-density limits / Jy	Sky Area / sr	Number of Sources	Uncertain redshifts	Spectroscopic completeness	Reference
3CRR	$S_{178} > 10.9$	4.24	170	0	100%	Laing et al. (1983)
6CE	$2.00 \leq S_{151} \leq 3.93$	0.10	58	7	97%	Rawlings et al. (2001)
6C*	$0.96 \leq S_{151} \leq 2.00$	0.13	29	6	100%	Jarvis et al. (2001a)

Table 1: Summary of the three samples used in the analysis to constrain the RLF of the most luminous radio sources. The spectroscopic completeness figure neglects uncertainties in a small number of redshifts in the 6CE and 6C* samples.

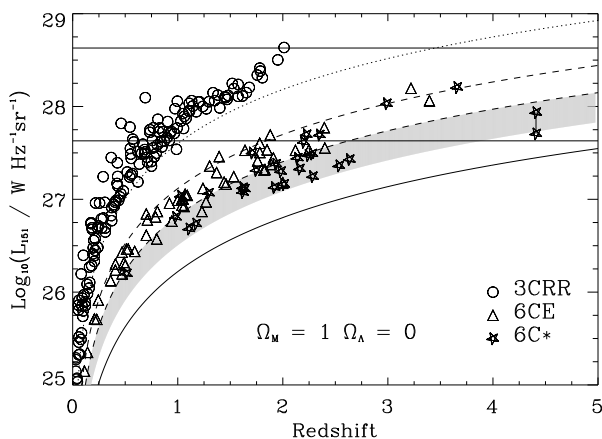


Figure 1: Rest-frame 151 MHz luminosity (L_{151}) versus redshift z plane for the three samples used in our analysis in cosmology I; 3CRR (circles), 6CE (triangles) and 6C* (stars). The rest-frame 151 MHz luminosity L_{151} has been calculated according to the polynomial fit to the radio spectrum described in Sec. 4.2. The 6C* source 6C*0140+326 at $z = 4.41$ is represented by two points joined by a solid vertical line. This is because 6C*0140+326 is thought to be subject to gravitational lensing by a foreground galaxy (Rawlings et al. 1996) and the highest luminosity point corresponds to the lensed luminosity whereas the lower point corresponds to the de-magnified, intrinsic luminosity of the source in the absence of significant lensing. The area between the horizontal lines is the region which contains the ‘most luminous’ sources according to our definition. The curved lines show the lower flux-density limit for the 3CRR (dotted) and 7CRS (solid). The dashed lines correspond to the limits for the 6CE sample and the shaded region shows the 6C* flux-density limits (all assuming a radio spectral index of 0.5). Note the area between the 3CRR sources and 6CE sources contains no sources, this is the area which corresponds to the absence of a flux-density-limited sample between the 6CE ($S_{151} \leq 3.93$ Jy) and 3CRR ($S_{178} \geq 10.9$ Jy) samples.

2.3 6CE

The 6CE sample originally defined by Eales et al. (1985), and recently revised by Rawlings et al. (2001), probes flux-densities a factor ~ 6 fainter than 3CRR. The sample consists of 59 objects, however, one of these (6CE1036+3616) is excluded for the statistically unbiased reason of there being a bright star occluding any likely optical identification. The sample considered here consists of 58 objects, with only two objects lacking a spectroscopic redshift, a completeness of $\sim 97\%$, with a further 7 redshifts not yet secure.

2.4 6C*

The 6C* sample (Blundell et al. 1998) is a filtered sample from part VI of the 6C survey of radio sources at 151 MHz which was designed to find radio sources at $z > 4$. The completeness of the sample is summarised in Table 1. At the faint flux-density limit of 6C*, the source counts of radio sources at 151 MHz are of order 10^4 per steradian, making it very difficult to construct a complete sample with spectroscopically determined redshifts over large solid angles. Moreover, the low-luminosity and thus low-redshift sources supply a significant contribution to the source counts at these flux-density limits making it increasingly difficult to use faint flux-density-limited samples to probe evolution of radio sources at high redshift. To combat this problem, additional selection criteria based on radio properties can be used to filter out the low-luminosity (low-redshift) sources. These additional selection criteria are discussed in detail in Blundell et al. (1998), but to summarise, only sources with spectral indices steeper than $\alpha_{0.151\text{G}}^{4.85\text{G}} \geq 0.981$, and angular size $\theta < 15$ arcsec are included. These selection criteria introduce additional complications in any analysis where the 6C* sample is used, and need to be treated with careful consideration as will be discussed in Sec. 4.1. This sample has now been reduced from 34 to 29 objects since images from the NVSS survey (Condon et al. 1998) have confirmed the suggestions of Blundell et al. (1998) that these objects were the hotspots of large ($\theta > 15''$) double sources. The optical spectroscopic follow-up of this sample has now been completed (Jarvis et al. 2001a)

and of the remaining objects, 23 have secure spectroscopic redshifts, and 6 have tentative redshifts. The redshifts of these six sources are typically based on a single definite emission line identified with a specific feature on the basis of a redshift estimate from the K -band magnitude.

It is also worth noting that the absence of strong Ly α emission in the objects from 6CE and 6C* which lack secure redshifts implies that these source are probably below $z \leq 1.8$, and should not affect the analysis in this paper (as we are only considering the most luminous sources which correspond to high redshifts at these flux-densities).

3 SELECTING ‘THE MOST LUMINOUS RADIO SOURCES’

The principal aim of this paper is to investigate the evolution in the comoving space density of steep-spectrum radio sources directly. Thus, we concentrate on only the ‘most luminous’ sources, which we are able to detect to $z \gtrsim 4$ in our flux-density-limited samples. Another reason for concentrating on just the most luminous objects is that in such a narrow luminosity range any bias from intrinsic correlations which are present in radio samples, such as luminosity - spectral index and linear size - spectral index correlations (e.g. Blundell et al. 1999) will be minimised. Selecting which sources from the three samples should be included in our analysis as the ‘most luminous’ was simply a question of where to place the lower limit in radio luminosity. To enable us to compare results between various cosmologies we are forced to alter the limits between cosmologies. Therefore to make the analyses consistent we only consider the top decade in L_{151} in cosmology I ($\Omega_M = 1$ and $\Omega_\Lambda = 0$). Thus all sources with $\log_{10} L_{151} \geq 27.63$ were included. For cosmology II ($\Omega_M = 0.3$ and $\Omega_\Lambda = 0.7$) we redefine our lower limit in luminosity at $\log_{10} L_{151} \geq 27.90$, this is not strictly the lower limit of the top-decade (which is $\log_{10} L_{151} \geq 27.95$) but allows the same number of sources into the modelling process as in cosmology I.

This selection process led to the inclusion of 57 3CRR sources for cosmology I and 55 3CRR sources for cosmology II, four (five) 6CE sources, and five (six) 6C* sources in cosmology I (cosmology II). These sources are tabulated in Table 2.

4 MODELLING THE RLF

4.1 6C* - what are we missing?

One of the principal problems in dealing with a filtered sample such as 6C* is determining which populations are filtered out. One of the aims of the 6C* sample was to find objects at $z > 4$. However, to use this sample

in any determination of how the comoving space density of radio sources evolves, we need to account for the sources excluded at all redshifts. This is crucial because if a significant number of sources between $2 \leq z \leq 3$ are filtered out of the sample, and objects at $z > 3$ are not, then on first inspection the results would be very misleading as the derived comoving space density at high redshift would be higher relative to the comoving space density at $z \sim 2$. To incorporate the effects of the selection criteria into the parametric modelling we adopt functional forms which parameterise the distributions in spectral shape and linear size, in addition to luminosity and redshift. These functional forms are described in the following sections.

4.2 Radio spectral shape

Many radio spectra are known to exhibit curvature (e.g. Laing & Peacock 1980; Blundell et al. 1999) thus rendering the use of a power-law spectral index inadequate in describing the radio spectra over a large frequency baseline. As a consequence of this, determining the rest-frame luminosity becomes less straightforward. Thus, to account for spectral curvature we fit the radio spectra with a polynomial of the form

$$y = \log_{10} S_\nu = \sum_{i=0}^N a_i x^i, \quad (1)$$

where $x = \log_{10}(\nu / \text{MHz})$. We fitted the flux-density data using a Bayesian polynomial regression analysis which assessed the posterior probability density function (pdf) for the required order of polynomial fit (e.g. Sivia 1996). This is the same method as used in Blundell et al. (1998) and Blundell et al. (1999). The results of this analysis are presented in Table 2; note that in no cases was $N > 2$ preferred, so the fits are either 1st or 2nd order polynomials.

4.3 Parametric modelling of the RLF for the most luminous radio galaxies and quasars

To extract as much information as possible from our dataset, we use three parametric models, with as few free parameters as possible, to estimate the RLF of the most luminous low-frequency-selected radio sources.

Following JR00 we construct a luminosity function separable in luminosity and redshift along with additional parameterisations describing the distributions in spectral shape and projected linear size.

We use a single power-law to parameterise the luminosity function $\rho_L(L_{151})$, i.e.

$$\rho_L(L_{151}) = \left(\frac{L_{151}}{L_o} \right)^{-\beta}, \quad (2)$$

where β is a dimensionless free parameter and L_o is a normalising luminosity fixed at the lower limit of the

Source	z	$\log_{10}(L_{151} / \text{WHz}^{-1}\text{sr}^{-1})$		a_1	a_2	D / kpc		Optical type
		Cos I	Cos II			Cos I	Cos II	
3C9	2.012	28.63	28.94	-0.47	-0.10	114.5	164.0	Q
3C13	1.351	28.06	28.33	-0.33	-0.11	241.7	330.8	G
3C14	1.469	28.07	28.35	-0.44	-0.08	205.5	284.1	Q
3C22	0.938	27.73	27.96	-0.58	-0.05	206.2	269.2	B
3C43	1.457	28.09	28.37	-0.75	0.00	21.4	29.6	Q
3C55	0.734	27.75	27.95	-0.09	-0.16	572.9	723.8	G
3C65	1.176	27.94	28.19	0.16	-0.18	149.7	201.4	S
3C68.1	1.238	28.00	28.26	-0.36	-0.10	447.9	606.4	Q
3C68.2	1.575	28.23	28.52	-0.39	-0.16	189.7	264.5	G
3C147	0.545	27.77	27.94	0.76	-0.22	22.1	26.8	Q
3C175	0.768	27.77	27.97	-0.92	-0.01	391.3	497.4	Q
3C181	1.382	28.12	28.39	-0.23	-0.11	49.0	67.2	Q
3C184	0.994	27.76	28.00	0.03	-0.16	40.8	53.7	G
3C186	1.063	27.89	28.14	0.18	-0.22	13.7	18.2	Q
3C190	1.197	28.04	28.30	-0.63	-0.04	57.7	77.8	Q
3C191	1.952	28.50	28.81	-0.78	-0.03	40.3	57.6	Q
3C196	0.871	28.35	28.58	-0.07	-0.13	83.6	108.0	Q
3C204	1.112	27.94	28.19	-1.18	0.01	314.2	419.6	Q
3C205	1.534	28.19	28.48	-0.34	-0.11	153.5	213.4	Q
3C208	1.109	28.03	28.28	-0.26	-0.13	94.4	126.1	Q
3C212	1.049	27.92	28.16	-0.78	0.00	77.0	102.0	Q
3C217	0.897	27.66	—	-0.33	-0.11	100.8	—	G
3C226	0.817	27.72	27.94	-0.52	-0.08	289.1	370.6	G
3C239	1.781	28.41	28.71	-0.48	-0.10	93.7	132.5	G
3C241	1.617	28.11	28.40	0.36	-0.24	7.7	10.8	G
3C245	1.029	27.84	28.08	-0.67	0.00	77.7	102.7	Q
3C252	1.105	27.95	28.20	-1.03	-0.01	514.9	687.1	G
3C254	0.734	27.72	27.92	-0.20	-0.14	105.7	133.5	Q
3C263.1	0.824	27.76	27.98	-0.21	-0.12	56.2	72.2	G
3C265	0.810	27.86	28.07	-0.82	-0.03	643.3	823.6	S
3C266	1.272	27.97	28.24	-0.34	-0.11	38.8	52.7	G
3C267	1.144	28.00	28.25	-0.60	-0.05	326.7	437.9	G
3C268.1	0.973	27.97	28.21	-0.70	0.00	390.5	512.4	G
3C268.4	1.400	27.98	28.26	-0.30	-0.10	93.6	128.7	Q
3C270.1	1.519	28.24	28.53	-0.96	0.02	102.5	142.2	Q
3C280	0.996	28.05	28.29	-0.50	-0.05	123.4	162.4	G
3C287	1.055	27.76	28.00	0.27	-0.13	0.8	1.0	Q
3C289	0.967	27.71	27.94	-0.14	-0.12	84.8	111.2	G
3C294	1.786	28.38	28.68	-0.82	-0.05	125.5	177.4	G
3C295	0.461	27.81	27.96	0.79	-0.26	37.7	44.9	G
3C309.1	0.904	27.83	28.06	-0.00	-0.10	24.4	31.7	Q
3C318	1.574	28.11	28.40	-0.01	-0.14	6.8	9.5	Q
3C322	1.681	28.20	28.49	-0.54	-0.07	278.6	391.2	G
3C324	1.206	28.05	28.31	-0.15	-0.14	86.1	116.2	S
3C325	0.860	27.72	27.95	-0.26	-0.10	133.4	172.2	G
3C336	0.927	27.71	27.94	-0.68	-0.03	183.1	238.7	Q
3C356	1.079	27.87	28.11	-0.50	-0.09	642.7	854.9	G
4C16.49	1.296	28.05	28.31	-1.00	0.00	137.8	187.6	Q
4C13.66	1.450	28.10	28.38	-0.81	0.00	51.4	71.0	G
3C368	1.132	28.06	28.31	-0.50	-0.13	67.9	90.9	G
3C380	0.691	28.09	28.29	-0.45	-0.04	158.8	199.0	Q
3C427.1	0.572	27.64	—	-0.57	-0.07	209.6	—	G
3C432	1.805	28.31	28.61	-0.38	-0.11	108.6	153.7	Q
3C437	1.480	28.12	28.40	-0.01	-0.13	294.3	407.4	G
3C454	1.757	28.33	28.63	-0.90	0.00	10.9	15.4	Q
3C469.1	1.336	28.14	28.42	-1.12	0.00	636.7	870.3	G
3C470.0	1.653	28.14	28.44	-0.39	-0.09	203.0	284.6	G
6CE0902+3419	3.395	28.06	28.41	-0.80	0.00	27.7	41.4	G
6CE0905+3955	1.880	27.69	27.99	-0.51	-0.10	920.4	1308.4	G
6CE0929+3855	2.394	27.77	28.09	-0.60	-0.05	28.9	42.2	G
6CE1204+3708	1.780	—	27.90	0.39	-0.22	—	609.2	G
6CE1232+3942	3.220	28.19	28.54	0.00	-0.21	54.4	81.2	G
6C*0020+440	2.988	28.03	28.37	-0.78	-0.05	72.9	108.1	G
6C*0032+412	3.658	28.20	28.56	-1.41	0.04	15.4	23.2	G
6C*0118+486	2.350	27.69	28.02	-2.01	0.16	126.7	184.2	G
6C*0135+313	2.199	—	27.93	-1.17	0.00	—	20.8	G
6C*0140+326	4.410	27.93	28.30	-0.07	-0.18	15.3	23.3	G
6C*0142+427	2.225	27.70	28.02	-1.38	0.05	121.4	175.5	G

Table 2: Sources selected from the 3CRR, 6CE and 6C* samples which correspond to our definition of the ‘most radio luminous’. The rest-frame 151 MHz luminosities were calculated by fitting a 1st or 2nd order polynomial to the available radio data as described in Sec. 4.2. The classes G, Q, B and S represent quasars, radio galaxies, broad-line radio galaxies and sources with scattered broad lines respectively, where we have followed the classifications of Willott et al. (1998) and Cos I and Cos II denote cosmologies I and II respectively. The solid horizontal lines are used where the source was not used for the specific cosmology due to it falling below our lower luminosity limit.

top-decade in luminosity, which is well above the ‘break’ luminosity in the RLF (Willott et al. 2001) and L_{151} is the rest-frame 151 MHz luminosity.

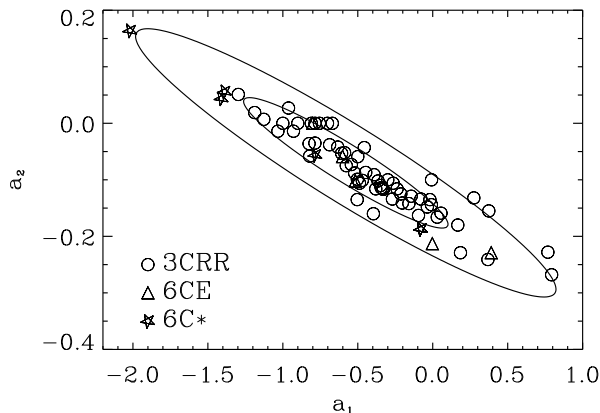


Figure 2: The correlated parameters a_1 and a_2 which describe the shape of the radio spectra. The circles are 3CRR sources; triangles correspond to 6CE sources and stars correspond to sources from the filtered 6C* sample. The inner (outer) contour corresponds to the 1σ (2σ) spread about the correlation using the best-fit value of model B in cosmology I.

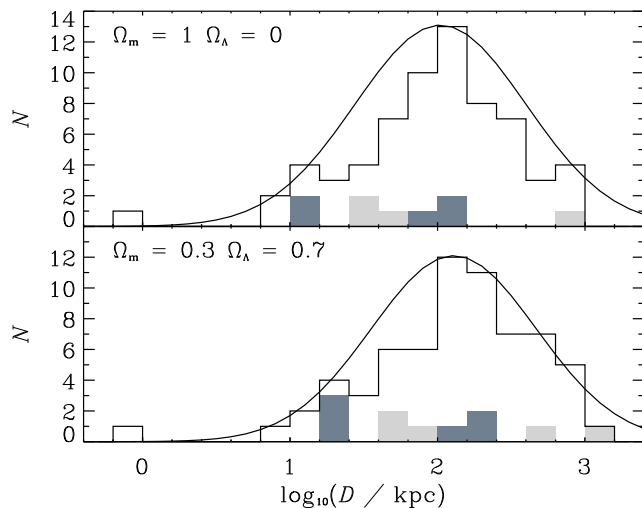


Figure 3: Histogram of the distribution in $\log_{10}(D/\text{kpc})$, where D is the projected linear size, for the top-decade in luminosity for cosmology I (top) and cosmology II (bottom). The white regions correspond to 3CRR sources, the light shaded regions are the contributions from the 6CE sample and the dark shaded regions are the 6C* sources. The solid line represents the Gaussian fit to the data from model A (Sec. 4.4) with an assumed normalisation factor which is incorporated within ρ_0 in the parametric modelling.

JR00 highlighted the importance of a distribution in spectral index in their parametric modelling and also

suggested that curvature would need to be incorporated in a full analysis of the RLF. The small number of sources in the JR00 sample restricted the models to a small number of free parameters and the effects of spectral curvature could not be incorporated into their parametric models. However, we are able to introduce a distribution for spectral curvature into the modelling of the RLF here, due to the larger number of sources in the top-decade of luminosity from our set of low-frequency-selected samples.

We fit the radio spectra with a polynomial of the form described in Sec. 4.2. Fig. 2 shows that the parameters describing spectral shape, a_1 and a_2 are linearly anti-correlated. Therefore to incorporate the effects of spectral curvature into the modelling of the RLF we use a functional form which accounts for this anti-correlation and the spread about it. To parameterise a_1 and a_2 we rotate the $a_1 - a_2$ plane by the free parameter ω to transform the correlation so it becomes parallel to the a_1 axis, i.e.

$$\begin{aligned} a'_1 - \mu_{a'_1} &= (a_1 - \mu_{a_1}) \cos(\omega) + (a_2 - \mu_{a_2}) \sin(\omega), \\ a'_2 - \mu_{a'_2} &= -(a_1 - \mu_{a_1}) \sin(\omega) + (a_2 - \mu_{a_2}) \cos(\omega), \end{aligned} \quad (3)$$

where a_1 and a_2 are defined in Sec. 4.2, a'_1 and a'_2 are the transformed coordinates of a_1 and a_2 rotated by the angle ω and $\mu_{a'_1}$ and $\mu_{a'_2}$ are the Gaussian peaks for the distributions in a'_1 and a'_2 respectively and are invariant with the rotation. We can now fit the distributions in both a'_1 and a'_2 with a Gaussian to characterise the spread about fitted mean values $\mu_{a'_1}$ and $\mu_{a'_2}$, i.e.

$$\rho_1(a'_1) = \exp \left\{ -\frac{1}{2} \left(\frac{a'_1 - \mu_{a'_1}}{\sigma_{a'_1}} \right)^2 \right\}, \quad (4)$$

and

$$\rho_2(a'_2) = \exp \left\{ -\frac{1}{2} \left(\frac{a'_2 - \mu_{a'_2}}{\sigma_{a'_2}} \right)^2 \right\}, \quad (5)$$

where $\mu_{a'_1}$ and $\mu_{a'_2}$ are as defined previously, and $\sigma_{a'_1}$ and $\sigma_{a'_2}$ are the characteristic widths of the Gaussians describing the distributions in a'_1 and a'_2 respectively. Thus, we obtain,

$$\rho_a(a_1, a_2) = \rho_1(a'_1) \rho_2(a'_2). \quad (6)$$

To account for the angular size filtering in 6C* we also require a functional form which characterises the distribution in projected linear size D . For this we assume that there are no correlations between D and the other parameters in the small luminosity range we consider[‡]. This enables us to model the linear size distri-

[‡] We note throughout this section that our chosen parameterisations are imperfect, e.g. there are likely to be weak correlations between radio spectral parameters, linear size and redshift even over a narrow range of radio luminosity (see BRW), but attempts to account for such subtleties would lead to an unacceptable in-

bution with a simple Gaussian distribution in $\log_{10} D$, i.e.

$$\rho_D(D) = \exp \left\{ -\frac{1}{2} \left(\frac{\log_{10} D - \log_{10} D_o}{\log_{10} D_1} \right)^2 \right\}, \quad (7)$$

where $\log_{10} D$ is the log of the projected linear size in kpc, $\log_{10} D_o$ is the peak of the Gaussian distribution and $\log_{10} D_1$ is the characteristic width of the Gaussian.

The final factor needed to model the distribution of sources is a component describing the redshift distribution of the most luminous radio sources. We use three independent models to achieve this.

Model A is parameterised as a single Gaussian distribution in redshift which is consistent with previous forms describing the evolution in the comoving space density from the literature (e.g. SH96), although as noted by JR00 this form has the disadvantage of being a symmetrical function, thus coupling the low-redshift evolution with the high-redshift evolution for which there is not necessarily any physical basis. For model A we take

$$\rho_A(z) = \exp \left\{ -\frac{1}{2} \left(\frac{z - z_o}{z_1} \right)^2 \right\}, \quad (8)$$

where z_o is the redshift of the Gaussian peak and z_1 is the characteristic width of the Gaussian.

Model B is a 1-tailed Gaussian which becomes constant beyond the Gaussian peak, this corresponds to a constant comoving space density above the Gaussian peak redshift, i.e.

$$\rho_B(z) = \begin{cases} \exp \left\{ -\frac{1}{2} \left(\frac{z - z_o}{z_1} \right)^2 \right\} & : z \leq z_o \\ 1.0 & : z > z_o, \end{cases} \quad (9)$$

where z_o and z_1 are as defined previously.

The third, and final model (C) uses a 1-tailed Gaussian to parameterise the low-redshift comoving space density and a power-law distribution at high redshift, i.e.

$$\rho_C(z) = \begin{cases} \exp \left\{ -\frac{1}{2} \left(\frac{z - z_o}{z_1} \right)^2 \right\} & : z \leq z_o \\ \left(\frac{1+z}{1+z_o} \right)^\eta & : z > z_o, \end{cases} \quad (10)$$

where z_o is the ‘break’ redshift where the model switches from the low- to the high-redshift form, z_1 is the characteristic width of the half-Gaussian and η is the power-law exponent describing the high-redshift comoving space density. This model has the advantage of being free to carry on increasing at high redshift, as we assume there is no *a priori* reason for a decline over the redshift range of interest. However, it has the disadvantage of an additional free parameter to the other

models. Note that model B is just model C with η fixed at zero.

The distribution for the complete radio luminosity function ρ , is thus given by the product of all these factors, i.e.

$$\rho(L_{151}, z, a_1, a_2, D) = \rho_o \times \rho_L(L_{151}) \times \rho_X(z) \times \rho_a(a_1, a_2) \times \rho_D(D), \quad (11)$$

where ρ_o is the normalising factor and a free parameter measured in units of Mpc^{-3} and $\rho_L(L_{151})$, $\rho_X(z)$ (for model X, where $X \in [A, B, C]$), $\rho_a(a_1, a_2)$ and $\rho_D(D)$ are dimensionless distribution functions per $(\Delta \log_{10} L_{151})$, per (Δz) , per $(\Delta a_1 \Delta a_2)$, and per $(\Delta \log_{10} D)$ respectively.

To find the best-fit values of the free parameters for the various models, the maximum likelihood method of Marshall et al. (1983) was used. If S is defined as $-2 \ln \mathcal{L}$, where \mathcal{L} is the likelihood function, then the aim is to minimise the value of S , which is given by:

$$\begin{aligned} S &= -2 \sum_{i=1}^N \ln[\rho(L_{151_i}, z_i, a_{1_i}, a_{2_i}, D_i)] \\ &+ 2 \iiint \iiint \rho(L_{151}, z, a_1, a_2, D) \\ &\times \Omega(L_{151}, z, a_1, a_2, D) \\ &\times \frac{dV}{dz} d(\log_{10} L_{151}) dz da_1 da_2 d(\log_{10} D), \end{aligned} \quad (12)$$

where $\rho(L_{151}, z, a_1, a_2, D)$ is the model distribution being tested, $\Omega(L_{151}, z, a_1, a_2, D)$ is the sky area available for the samples under consideration in this paper for a given flux-density, and (dV/dz) is the differential comoving volume element. The first term is simply the sum over N sources in the defined sample. The second term is the integral of the model distribution being tested and should give $\approx 2N$ for good fits.

The lower and upper limits of the integral are $27.63 \leq \log_{10} L_{151} \leq 28.63$ for cosmology I, and $27.90 \leq \log_{10} L_{151} \leq 28.95$ for cosmology II, $0 < z < 10$, $-2.2 \leq a_1 \leq 1.0$, $-0.4 \leq a_2 \leq 0.2$ and $-0.3 \leq \log_{10} D \leq 4.0$. To illustrate the goodness-of-fit of the models the 2-dimensional Kolmogorov-Smirnov (KS) test, originally proposed by Peacock (1983) was used in the form of Press et al. (1992). The KS-test enables one to determine the probability, P_{KS} , that a model distribution is a true representation of the dataset. However, the 2D KS-test may only be used to reject models, it cannot determine how well a model fits. Indeed, when the probability, $P_{KS} > 0.2$, its value may not be accurate but the implication that the model and data are similar is still correct. For this reason, the relative probability of each model, P_R , is also evaluated directly from the minimisation algorithm.

Model	Cosmology I			Cosmology II		
	A	B	C	A	B	C
N	11	11	12	11	11	12
$\log_{10} \rho_{\circ}$	-6.98 ± 0.12	-7.08 ± 0.13	-7.10 ± 0.12	-7.26 ± 0.10	-7.33 ± 0.11	-7.31 ± 0.14
β	2.00 ± 0.18	2.07 ± 0.10	1.98 ± 0.18	2.21 ± 0.17	2.21 ± 0.24	2.20 ± 0.20
z_{\circ}	2.76 ± 0.22	2.10 ± 0.23	2.05 ± 0.30	2.76 ± 0.24	2.12 ± 0.24	2.15 ± 0.30
z_1	1.00 ± 0.13	0.74 ± 0.16	0.70 ± 0.17	0.94 ± 0.13	0.65 ± 0.14	0.67 ± 0.15
η	—	—	0.10 ± 1.33	—	—	-0.06 ± 1.53
ω	-0.16 ± 0.01	-0.16 ± 0.01	-0.16 ± 0.01	-0.16 ± 0.01	-0.16 ± 0.01	-0.16 ± 0.01
$\mu_{a'_1}$	-0.56 ± 0.07	-0.55 ± 0.07	-0.54 ± 0.07	-0.58 ± 0.07	-0.59 ± 0.07	-0.59 ± 0.08
$\sigma_{a'_1}$	0.50 ± 0.05	0.49 ± 0.05	0.49 ± 0.05	0.49 ± 0.04	0.50 ± 0.05	0.49 ± 0.04
$\mu_{a'_2}$	-0.07 ± 0.01	-0.07 ± 0.01	-0.07 ± 0.01	-0.07 ± 0.01	-0.07 ± 0.01	-0.07 ± 0.01
$\sigma_{a'_2}$	0.027 ± 0.003	0.027 ± 0.002	0.027 ± 0.002	0.026 ± 0.002	0.026 ± 0.002	0.026 ± 0.002
D_{\circ}	2.04 ± 0.07	2.02 ± 0.07	2.00 ± 0.08	2.12 ± 0.07	2.11 ± 0.07	2.12 ± 0.07
D_1	0.59 ± 0.06	0.58 ± 0.05	0.59 ± 0.06	0.56 ± 0.05	0.56 ± 0.05	0.56 ± 0.05
S_{\min}	2803.1	2799.8	2798.5	2941.7	2936.7	2936.6
$\ln \sqrt{\text{Det}(\nabla\nabla S)}$	40.8	39.3	40.5	41.1	38.9	40.1
P_{R}	0.04	1.00	1.11	0.01	1.00	0.32

Table 3: Best-fit parameters for the model RLFs described in Sec. 4.3 along with their associated 1σ errors. N is the number of free parameters for each model, S_{\min} is the minimum value of eqn. 12, $\text{Det}(\nabla\nabla S)$ is the determinant of the Hessian matrix evaluated at $S = S_{\min}$ and P_{R} is the relative probability of the models with respect to model B. A detailed description of how the errors and relative probabilities are ascribed can be found in JR00.

4.4 Results of the parametric modelling

Table 3 shows the best-fit parameters for the various models: S_{\min} is the minimum of eqn. 12 and P_{R} is the relative probability with respect to model B. The parameter describing the slope of the luminosity function β is consistent with the previous results of DP90 and Willott et al. (2001) for the steep-spectrum RLF and Willott et al. (1998) for the RLF of steep-spectrum quasars. A 2D KS-test to the predicted $L_{151} - z$ plane from the best-fit parameters give $0.2 \leq P_{\text{KS}} \leq 0.4$ for all of our models in both cosmologies suggesting good working models. The best-fit values for the correlation between a_1 and a_2 are consistent over all models in the two cosmologies and are also statistically reasonable with a 2-D KS-test giving $P_{\text{KS}} = 0.31$ (Fig. 2). The parameters describing the Gaussian distribution in $\log_{10} D$ also span a narrow range between models and KS-probabilities of $P_{\text{KS}} \approx 0.56$ (cosmology I) and $P_{\text{KS}} \approx 0.34$ (cosmology II) suggests adequate fits to the data for all models. The histogram of $\log D / \text{kpc}$ and the fitted Gaussian are shown Fig. 3.

The parametric models show that model B, with a constant comoving space density above a critical redshift is ~ 20 (~ 100) times more likely than model A, the model with a symmetric Gaussian decline in cosmology I (cosmology II). However, one may associate these relative probabilities with the forced symmetry in model A, thus forcing a poorer fit at either low- or at high-redshift and these models must be considered with

this property in mind. The best-fit parameters of model C are probably more relevant in discriminating between models with sharp cut-offs and those with constant or increasing space densities.

Model C uses a 1-tailed Gaussian up to a critical redshift and a power-law exponent beyond this critical redshift, thus decoupling the low-redshift from the high-redshift space density. However, this model requires one more free parameter than models A and B. This introduces an additional factor when calculating the relative likelihood of this model, which is described in detail in JR00. [§] The best-fit model suggests that there is very little evidence for an abrupt decline in the comoving space density of the most luminous low-frequency-selected sources at high redshift. Indeed the best-fit to the power-law exponent in cosmology I (Table 3) suggests a steady increase up to an indeterminable redshift, and the best-fit in cosmology II is a power-law exponent of ~ 0 thus giving a constant comoving space density, albeit with an uncertainty encompassing moderate de-

[§] On the assumption that most of the prior ranges cancel on dividing the probabilities of model A and model B, this additional factor is given by,

$$\mathcal{F} = (4\pi)^{\frac{11-N}{2}} \Delta\eta, \quad (13)$$

where N is the number of free parameters and the 11 arises from the number of free parameters in the comparison model (B), and $\Delta\eta$ is the prior range of the additional parameter. The factor \mathcal{F} is of order unity and has been neglected for our analysis here.

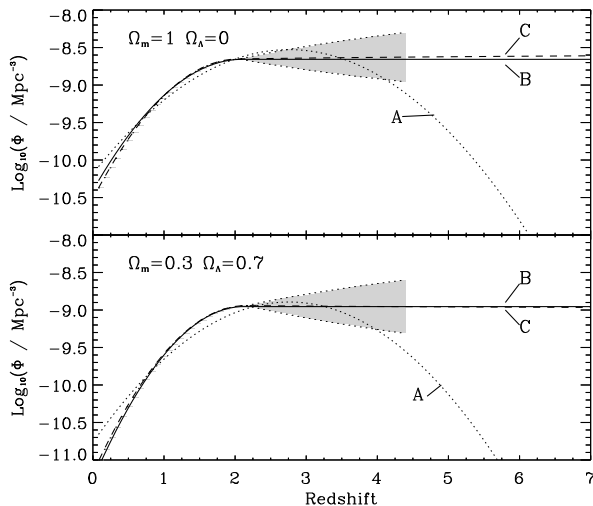


Figure 4: The comoving space density Φ [$\int \int \int \int \rho d(\log_{10} L_{151}) dz da_1 da_2 d(\log_{10} D)$] of the most luminous low-frequency-selected radio sources using the three models described in Sec. 4.3 for both cosmology I (top) and cosmology II (bottom). The dotted line is from the best-fit parameters of model A; the solid line for model B; and the dashed line represents model C. The shaded region corresponds to the 1σ uncertainty for the power-law exponent of model C. This confidence region is uncertain beyond the limit of our dataset and thus we have excluded it at $z > 4.41$, i.e. beyond the highest redshift source in our samples, although as the redshift distribution in Sec. 6 shows, these uncertainties have very little influence on the high-redshift evolution due to the lack of available comoving volume.

clines and inclines. This uncertainty on the power-law exponent η is represented by the shaded region in Fig. 4 and also by a probability distribution function (pdf) in Fig. 5 and it is obvious that there exists a large range in which η may reside. This behaviour is different from the pdf for the power-law exponent from the parametric modelling of the flat-spectrum population of JR00 at $\approx 2 - 3\sigma$ level, where the pdf derived from the V/V_{\max} method peaked at $\eta \approx -3$, which is also consistent with their best-fit parametric models.

The dissimilarity between the behaviour observed by JR00 for the most luminous flat-spectrum sources from a high-frequency selected sample, where there was $\sim 2\sigma$ evidence for a decline by a factor of ~ 4 between $2.5 \leq z \leq 5$, and this analysis is resolvable within the large uncertainties. Although the steep decline ruled out at the 2σ level for flat-spectrum sources in JR00 is ruled out at roughly the 4σ level here. However, if the difference in the best-fit power-law exponents is a real difference between the two radio source populations then it may not necessarily be due to a breakdown of

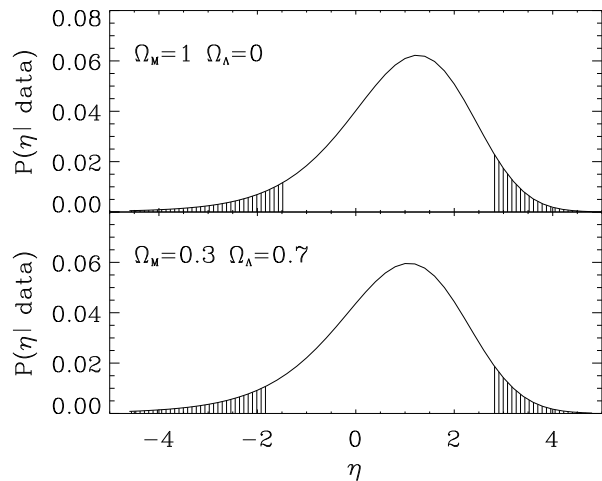


Figure 5: The probability density function for the power-law exponent η of model C for both cosmology I (top) and cosmology II (bottom), normalised such that the area under the curve is unity. The pdf was determined by marginalising over the free parameters ρ_o , β , z_o and z_1 , i.e. the four parameters with the largest uncertainties from the modelling (all other parameters were fixed at their best-fit values). The unshaded region corresponds to the 90% confidence region.

orientation-based unified schemes and we will discuss this in Sec. 7.

4.5 The effect of changing the lower luminosity limit

We now investigate the effect that the positioning of the lower limit in radio luminosity has on the outcome of the parametric modelling. Each model was re-fitted with both the lower-limit in radio luminosity increased by 0.25 dex and also lowered by 0.25 dex. The relative probabilities of the best-fit models in both cosmologies changed very little with this alteration. The uncertainties on the fitted parameters increased when the luminosity limit was raised, as one might expect due to the small number statistics becoming increasingly important. The steepness of the RLF, governed by the β parameter in our models was consistently ≈ 2.1 within the uncertainties, suggesting that the steepness of the RLF in the high-luminosity regime is consistent with β at lower luminosities. The power-law exponent η for the high-redshift evolution in model C also varied very little from a best-fit value of ≈ 0 , although the large errors associated with this parameter still make shallow declines and also shallow increases easily plausible. Therefore, we conclude that the positioning of the lower-limit in radio luminosity has an insignificant effect on the relative probabilities and the fitted values of the parametric modelling if the modelling is restricted to only the most

radio luminous sources, where we are confident of completeness in all of the samples.

To test the susceptibility of our models to small number statistics we also re-fitted our models with an additional *fake* $z = 6$ source. Inclusion of the $z = 6$ radio source in our models also has very little effect on the relative probabilities, although model A becomes slightly less plausible relative to model B in both cosmologies as one would expect. The η parameter is still consistent with a value of $\eta \approx 0$ and no positive evolution in the comoving space density is required (although the best-fit values are $\eta = 0.35$ and $\eta = 0.20$ for cosmology I and II respectively). The peak of the low-redshift Gaussian is constrained at a value of $z_o \sim 2$, although the errors on this parameter are high and correlated with the η parameter. We therefore conclude that including a radio galaxy at $z = 6$ has little effect on the overall conclusions of our main analysis, as the small number statistics involved in including a single source at high redshift are easily compatible with the original best-fit models without the $z = 6$ source. This is also highlighted by the predicted redshift distribution from our original model C (Fig. 7), where the presence of a single source at $z \sim 6$ could easily conform to the predictions in both cosmologies.

5 THE BANDED V/V_{MAX} STATISTIC

It is also useful to view our parametric modelling along with a non-parametric form in which the behaviour in the space density of the most luminous, high-redshift sources does not depend on the assumed parameterisation. The most common method for this non-parametric analysis is the V/V_{MAX} method in its banded form (Avni & Bahcall 1980; see also DP90, and JR00). Unfortunately, with a filtered sample such as 6C* the actual significance of any value of $V/V_{\text{MAX}} > 0.5$ may be viewed as inconsequential due to the bias towards finding objects at high redshift. However, if this banded test shows a significant decline in the comoving space density of sources with a sample biased to finding objects at high redshift then it would prove to be a significant detection of any redshift cut-off. Fig. 6 shows the banded V/V_{MAX} statistic for all of the sources in the top-decade in radio luminosity considered in our parametric modelling. It is apparent that the statistic shows no significant evidence for a decline in the comoving space density out to $z \sim 4.5$, if the highest-redshift (lensed) radio galaxy 6C*0140+326 is included. If we now repeat the analysis without this object there also appears to be little evidence of a decline, with all points lying within 1σ of the line of no-evolution at $V/V_{\text{MAX}} = 0.5$. Therefore, we find no evidence for a decline in the comoving space density of the most luminous radio sources using this non-parametric approach, in agreement with the best-fits from our parametric models. The high values

of V/V_{MAX} in Fig. 6 reflect a combination of genuine positive evolution at $z < 2$ as the 3CRR sources dominate in this regime, and biases due to selection methods at higher redshifts where the sample becomes increasingly dominated by 6C*.

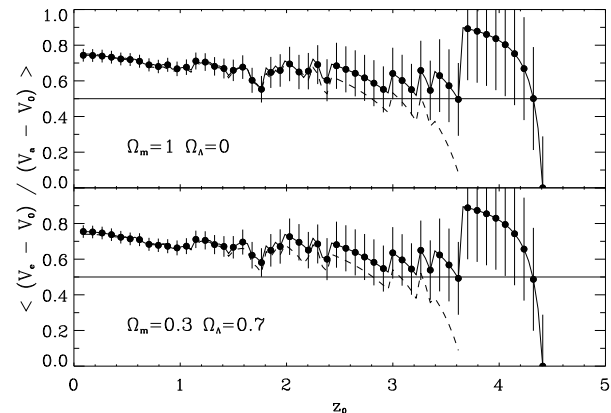


Figure 6: The banded V/V_{MAX} statistic for the most radio luminous steep-spectrum sources considered in this paper. The solid line corresponds to the statistic with the lensed radio galaxy 6C*0140+326 included in the analysis and the dashed line is the statistic excluding this source. The solid vertical lines correspond to the 1σ errors on the statistic assuming $\sigma = 1/\sqrt{12N}$ (Avni & Bahcall 1980), where N is the number of sources above z_o .

6 PREDICTED REDSHIFT DISTRIBUTIONS

We now consider the redshift distribution expected given our best-fit values for model C. Fig. 7 shows the cumulative redshift distribution for our sample for $z > 2$, along with the predicted distribution for model C from our best-fit model. The forced symmetry in the estimation of these errors by fitting a symmetrical Gaussian to the minima in the parametric modelling (see JR00) means that the uncertainties may be overestimated on one side and underestimated on the other. Therefore, although the predicted redshift distributions are in accord with the data the actual 1σ errors may not be telling us the whole story. Thus, the pdf shown in Fig. 5 is probably a better representation of the uncertainties in the parameter space we are most interested in. We can see that the model parameters are consistent with the data all the way through the high redshift regime. The upper limit on the η parameter from our 1σ uncertainty is easily consistent with the data. This highlights the effect of the small number statistics under consideration at the highest redshifts. The steepness of the RLF, combined with the sharp reduction in the available comoving volume due to the flux-density limits

of the samples means that, even without any decline in the comoving space density of radio sources, the number of sources one would expect to find is < 1 .

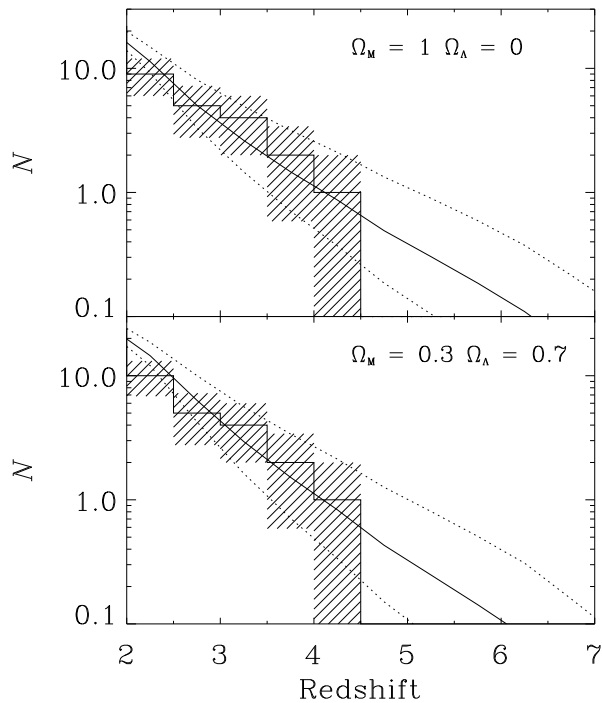


Figure 7: Cumulative redshift distributions at $z > 2$ for model C in cosmology I (top) and cosmology II (bottom). The histogram represents the actual cumulative redshift distribution of the sources in the 3 samples used, the hashed regions are the \sqrt{N} errors on the binned data. The solid curve is the predicted distribution from the best-fit values of model C. The two dotted curves represent the curves for the 1σ uncertainty on the high-redshift exponent η , using the uncertainties generated in our parametric modelling.

7 THE RLF OF STEEP- AND FLAT-SPECTRUM RADIO SOURCES IN THE CONTEXT OF UNIFIED SCHEMES

Our work on the radio luminosity function of both steep-spectrum radio sources (this paper) and flat-spectrum radio sources (JR00) has highlighted the difficulty in establishing the comoving space density of these sources at redshifts which push to the limits of flux-density-limited radio samples. Although the uncertainties on the fitted parameters describing the high-redshift behaviour of both these types of radio source are quite large they are markedly different in their mean value for the high-redshift power-law exponent. Indeed the evidence from our parametric modelling favours a steady decline for the flat-spectrum population by a factor ~ 4 between $2.5 \leq z \leq 5$ (JR00), whereas analysis

of the low-frequency samples in this paper lead us to a best-fit model with a roughly constant comoving space beyond a peak redshift around $z \approx 2.5$.

This discrepancy is just resolvable within the uncertainties of both models, so it is plausibly a statistical fluke that we are seeing different evolutionary behaviour between the two populations of radio sources. However, other plausible explanations exist and should be investigated further.

The most obvious difference between the flat- and steep-spectrum samples is the selection frequency. The high selection frequency (2.7 GHz) for the flat-spectrum sample means that the majority of objects are core-dominated Doppler-boosted quasars and, as argued by JR00, Giga-Hertz Peaked spectrum (GPS) sources may also make an important contribution. If a significant fraction of the most luminous flat-spectrum sources are indeed GPS sources, then at an observed frequency of 2.7 GHz, the radio spectrum of a GPS source may have steepened by an amount sufficient for it to drop below the sample flux-density limit or for it to have been rejected from the sample on account of its steep observed spectral index ($\alpha > 0.5$) if it is at high redshift. Indeed even if the core-dominated, Doppler-boosted sources are a dominant part of the top-decade of the flat-spectrum luminosity function, and assuming a conservative estimate for the fraction of GPS sources, a decline in the comoving space density would be observed at high redshift. This is because of the drop off in GPS sources due to K-correction effects, allowing a roughly constant comoving population of Doppler-boosted sources. This point was made by JR00 and they suggest a model for the RLF is needed in which both the Doppler-boosted and GPS populations are explicitly considered. The banded V/V_{\max} method used by JR00 was able to account for the spectral shape of individual sources and although small number statistics make it very difficult to be certain (see the broad 90% confidence region in their Fig.9b), the presence of some high-redshift decline in one or more of the Doppler-boosted and GPS populations appears robust to spectral-dependent selection effects.

Another difference between the flat- and steep-spectrum sources is the steepness of the luminosity function in the top decade. JR00 found values in the range $1.2 \leq \beta \leq 1.75$ for the top decade of the flat-spectrum population, whereas values of $\beta \geq 2.0$ have been determined for the top decade of steep-spectrum RLF in this analysis and over a broader range in luminosities in previous work (e.g. Willott et al. 1998; Willott et al. 2001). DP90 also found a marginally steeper luminosity function for their steep-spectrum population ($\beta \sim 2.2$) compared to their flat-spectrum sample ($\beta \sim 2.0$).

The difference in both the high-redshift decline and values of β between the flat- and steep-spectrum sources can be resolved by considering the concave shape of the RLF (Willott et al. 2001). The most lumi-

nous flat-spectrum population probes a different part of the underlying RLF than the most luminous low-frequency-selected sources (JR00). Thus, if the position of high-frequency selected flat-spectrum sources on the underlying RLF are at luminosities which are lower than those of the most luminous low-frequency-selected sources and lie on or near the ‘break’ in the RLF at $\log_{10} L_{151} \sim 26.5$ for cosmology I (Willott et al. 2001), then this automatically supports the steeper values derived for β from our steep-spectrum samples. In other words, the slope in the RLF steepens with increasing intrinsic luminosity, so either Doppler boosted or GPS sources in high-frequency samples will be drawn from a population where the slope in the underlying RLF is flatter. Indeed, it seems likely that the Doppler boosted and GPS objects are drawn from different points on the underlying RLF, so there may well be differential effects: JR00 for example, have suggested this as the cause of an increasing fraction of GPS sources with increasing luminosity in high-frequency selected, flat-spectrum samples.

The difference in the evolution of high-redshift comoving space density between the flat- and steep-spectrum populations can now be understood if there is a decline in the comoving space density at high redshift for lower-luminosity low-frequency sources. This would be very important to confirm because the luminosity density ($\int L\rho d\log_{10}L$) of the population is dominated by the space density near the break of the RLF. It is impossible to probe this break region directly with the complete flux-density-limited samples currently available.

We therefore conclude that, although the high-redshift space density and the steepness of the RLF may be different for flat- and steep-spectrum sources in the top-decade of luminosity, this can easily be explained by some combination of two effects: first, a mixed population of Doppler boosted and GPS sources in the high-frequency selected flat-spectrum samples; second, and arguably more importantly, the flat- and steep-spectrum populations lie on different parts of an underlying RLF which is concave (Willott et al. 2001). Thus, orientation-based unified schemes are not challenged by the comparison of constraints on the high-redshift evolution of flat- and steep-spectrum radio sources.

8 CONCLUSIONS

The main conclusions we have drawn from our parametric modelling analysis of the most luminous low-frequency-selected radio sources are:

- Their low-redshift evolution follows the same track as that of flat-spectrum radio sources, optically selected AGN (e.g. Schmidt, Schneider & Gunn 1995) and X-ray selected AGN (e.g. Miyaji, Hasinger & Schmidt 2000),

with an increase in comoving space density by a factor $\gtrsim 100$ over $0 \leq z \leq 2.5$.

- Their steep increase in space density slows down at $z > 2.5$ in spatially-flat cosmologies with either $\Omega_{\Lambda} = 0$ or $\Omega_{\Lambda} = 0.7$.

- The saturated Gaussian model B with a constant comoving space density beyond a peak redshift, is ≈ 25 (≈ 100) times more likely than model A with a Gaussian rise and cut-off for cosmology I (II). Although this ratio may partly reflect the forcing of the low-redshift increase to be symmetric with the high-redshift decline in the comoving space density of the most luminous radio sources, it does illustrate the significant difference between radio-loud AGN and optically selected quasars [which do have a roughly Gaussian evolutionary behaviour, e.g. Schmidt et al. (1995); Kenefick, Djorgovski & de Carvalho (1995)].

- The best-fit model is consistent with a constant comoving space density beyond the peak at $z \approx 2.5$ to an indeterminable redshift, although the uncertainties span a wide range covering both moderate declines and continuing shallow inclines.

- The difference between the high-redshift space density for flat- and steep-spectrum sources is marginally significant, although there remain worries concerning the mixture of Doppler Boosted and GPS sources in the flat-spectrum population. An explanation exists in which the high-frequency flat-spectrum sources are probing the underlying RLF at fainter intrinsic luminosities than the top-decade discussed in this paper. This could also resolve the difference in β between the two populations, because at lower-luminosities the sources are edging towards the break in the luminosity function where β becomes flatter (Willott et al. 2001). This is important to confirm since the tentative evidence for a decline in the flat-spectrum population supplies indirect evidence of a decline in the luminosity density in the radio source population at high redshift.

ACKNOWLEDGEMENTS

We are grateful to a large number of colleagues who have devoted effort and observing time to the quest for redshifts for the 6CE and 6C* samples. This research has made use of the NASA/IPAC Extra-galactic Database, which is operated by the Jet Propulsion Laboratory, Caltech, under contract with the National Aeronautics and Space Administration. MJJ thanks PPARC for the receipt of a studentship.

REFERENCES

- Antonucci R.R.J., 1993, ARAA, 31, 473
 Avni Y., Bahcall J.N., 1980, ApJ, 235, 694
 Barthel P.D., 1989, ApJ, 336, 606
 Blundell K.M., Rawlings S., 1999, Nature, 399, 330

- Blundell K.M., Rawlings S., Eales S.A., Taylor G.B., Bradley A.D., 1998, MNRAS, 295, 265
- Blundell K.M., Rawlings S., Willott C.J., 1999, AJ, 117, 677
- Condon J.J., Cotton W.D., Greisen E.W., Yin Q.F., Perley R.A., Taylor G.B., Broderick J.J., 1998, AJ, 115, 1693
- Condon J.J., Helou G., Sanders D.B., Soifer B.T., 1990, ApJS, 73, 359
- Dunlop J.S., Peacock J.A., 1990, MNRAS, 247, 19
- Eales S.A., 1985, MNRAS, 217, 149
- Eales S.A., Rawlings S., Law-Green, D., Cotter, G., Lacy, M., 1997, MNRAS, 291, 593
- Jackson C.A., Wall J.V., 1999, MNRAS, 304, 160
- Jarvis M.J., Rawlings S., 2000, MNRAS, 319, 121
- Jarvis M.J. et al., 2001a, MNRAS in press (astro-ph/0106127)
- Jarvis M.J., Rawlings S., Eales S.A., Blundell K.M., Bunker A.J., Croft S.D., McLure R.J., Willott C.J., 2001b, MNRAS in press (astro-ph/0106130)
- Kennefick J.D., Djorgovski S.G., de Carvalho R.R., 1995, AJ, 110, 2553
- Laing R.A., Peacock J.A., 1980, MNRAS, 190, 903
- Laing R.A., Riley J.M., Longair M.S., 1983, MNRAS, 204, 151
- Longair M.S., 1966, MNRAS, 133, 421
- Marshall H.L., Avni Y., Tanenbaum H., Zamorani G., 1983, ApJ, 269, 35
- Miyaji T., Hasinger G., Schmidt M., 2000, A&A, 353, 25
- Peacock J.A., 1983, MNRAS, 202, 615
- Peacock J.A., 1985, MNRAS, 217, 601
- Press W.H., Teukolsky S.A., Vetterling W.T., Flannery B.P., 1992, Numerical Recipes: The Art of Scientific Computing. CUP, Cambridge
- Rawlings S., Blundell K.M., Lacy M., Willott C.J., Eales S.A., 1998, in *Observational Cosmology with the New Radio Surveys*, eds. M.N. Bremer et al., 171, Kluwer
- Rawlings S., Eales S.A., Lacy M., 2001, MNRAS, 322, 523
- Rawlings S., Lacy M., Blundell K.M., Eales S.A., Bunker A.J., Garrington S.T., 1996, Nature, 383, 502
- Sandage A., 1972, ApJ, 178, 25
- Schmidt M., Schneider D.P., Gunn J.E., 1995, AJ, 110, 68
- Shaver P., Hook I.M., Jackson C.A., Wall J.V., Kellermann K.I., 1998, in *Highly Redshifted Radio Lines*, eds. C.Carilli, S.Radford, K.Menten & G.Langston (astro-ph/9801211)
- Shaver P.A., Wall J.V., Kellermann K.I., Jackson C.A., Hawkins M.R.S., 1996, Nature, 384, 439
- Sivia D.S., 1996, *Data Analysis: A Bayesian Tutorial*, OUP
- Willott C.J., Rawlings S., Blundell K.M., Lacy M., 1998, MNRAS, 300, 625
- Willott C.J., Rawlings S., Blundell K.M., Lacy M., 2000, MNRAS, 316, 449
- Willott C.J., Rawlings S., Blundell K.M., Lacy M., Eales S.A., MNRAS, 2001, 322, 536